JACS
JOURNAL OF THE AMERICAN CHEMICAL SOCIETY
pubs.acs.org/JACS
Article

Bifunctional Electron-Transporting Agent for Red Colloidal Quantum Dot Light-Emitting Diodes

Ya-Kun Wang,[#] Haoyue Wan,[#] Jian Xu,[#] Yun Zhong,[#] Eui Dae Jung, So Min Park, Sam Teale, Muhammad Imran, You-Jun Yu, Pan Xia, Yu-Ho Won, Kwang-Hee Kim, Zheng-Hong Lu, Liang-Sheng Liao, Sjoerd Hoogland, and Edward H. Sargent*

Cite This: https://doi.org/10.1021/jacs.2c13677

ABSTRACT: Indium phosphide (InP) quantum dots have enabled light-emitting diodes (LEDs) that are heavy-metal-free, narrow in emission linewidth, and physically flexible. However, ZnO/ZnMgO, the electron-transporting layer (ETL) in high-performance red InP/ZnSe/ZnS LEDs, suffers from high defect densities, quenches luminescence when deposited on InP, and induces performance degradation that arises due to trap migration from the ETL to the InP emitting layer. We posited that the formation of Zn^{2+} traps on the outer ZnS shell, combined with sulfur and oxygen vacancy migration between ZnO/ZnMgO and InP, may account for this issue. We synthesized therefore a bifunctional ETL (CNT2T, 3′,3′″,3′″″-(1,3,5-triazine-2,4,6-triyl)tris(([1,1′-biphenyl]-3-carbonitrile)) designed to passivate Zn^{2+} traps locally and *in situ* and to prevent vacancy migration between layers: the backbone of the small molecule ETL contains a triazine electron-withdrawing unit to ensure sufficient electron mobility (6×10^{-4} cm^2 V^{-1} s^{-1}), and the star-shaped structure with multiple cyano groups provides effective passivation of the ZnS surface. We report as a result red InP LEDs having an EQE of 15% and a luminance of over 12,000 cd m^{-2}; this represents a record among organic-ETL-based red InP LEDs.

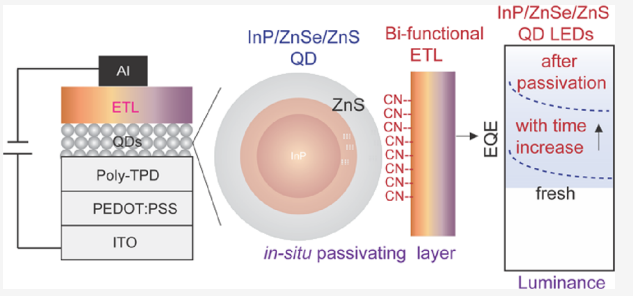

INTRODUCTION

Colloidal quantum dot light-emitting diodes (QD LEDs) unite color purity, structural diversity, tunable band gap, and low-cost solution processing for displays.[1−5] Emission results from recombination of charge carriers injected from the hole and electron transport layers. The electron-transporting layer (ETL) is relatively understudied, with material systems primarily focused on inorganic metal oxides (ZnMgO, ZnO, and SnO_2).[6−8]

InP/ZnSe/ZnS core−shell-based LEDs provide a heavy-metal-free route to efficient LEDs.[9,10] High-performance red InP LEDs (external quantum efficiency, EQE > 15%) have been achieved by optimizing their ZnMgO or ZnO ETLs; however, performance drops to <15% when using other ETL materials.[11−14] ZnO/ZnMgO ETLs suffer from defects and severe quenching: the deposition of these ETLs on InP induces a photoluminescence quantum yield (PLQY) drop and LED degradation due to trap migration from the ETL to the emitting layer.[15,16] Inserting an extra passivation layer between ZnMgO ETL and emitter can partially relieve the PLQY drop and device degradation,[17−19] but this needs delicate thickness control to the monolayer limit to minimize the conductivity barrier, complicating the fabrication process.

Organic and organic−inorganic hybrid ETL systems address the PLQY quenching issue in ZnMgO/ZnO ETLs, but the mismatched band alignment and low conductivity of these ETL systems impose restrictions that result in inferior EQEs.[11,12] Various ETLs have been proposed to improve the performance of red InP LEDs, but these either exhibit inferior efficiency (<15%)[20] or need complicated fabrication processes that include double ETL layer evaporation and delicate thickness control.[21] Developing new ETL systems to replace ZnO/ZnMgO in efficient InP LEDs represents an important challenge for the field.

We investigated trap states in InP/ZnSe/ZnS core−shell QDs and identified the role of the ZnS shell, where a Zn^{2+} vacancy forms and S^- migrates to the ETL layer (Figure 1a). We found out that this accelerates PL quenching, leading it to become more severe during photogeneration and under applied bias. We posited that a bifunctional agent could address this challenge if it included an electron-deficient backbone ensure the needed electron mobility, united with electron-rich units to bind to Zn^{2+} to passivate surface traps

Received: December 22, 2022

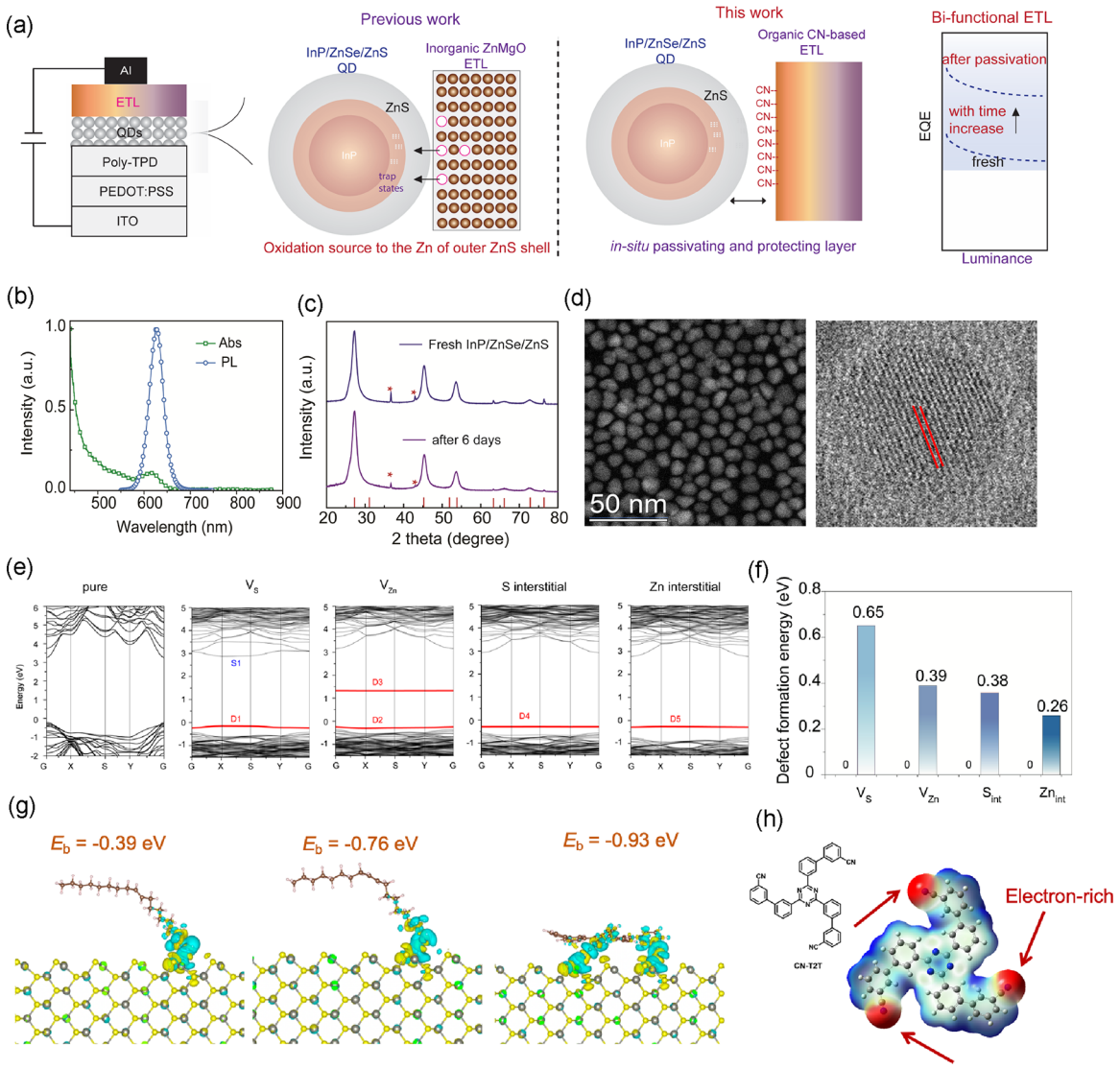

Figure 1. Bifunctional ETL to passivate and protect InP/ZnSe/ZnS QDs in LEDs. (a) Previously reported InP LED architecture with a ZnMgO ETL and this work using a CNT2T ETL to passivate and protect the InP active layer; (b) absorption and photoluminescence of the InP; (c) XRD of fresh InP/ZnSe/ZnS films and after aging in air for 6 days (the bottom red lines indicate simulated XRD from single crystal InP); (d) high-resolution TEM images of the InP; (e) band structure and defect level analysis for V_S, V_{Zn}, S_{int}, and Zn_{int}; (f) relative defect formation energy of V_S, V_{Zn}, S_{int}, and Zn_{int} on a ZnS (110) surface with CNT2T adsorbed, with reference to the pure system; (g) charge density difference and binding energy values (to Zn^{2+} traps) of CNT2T (−0.93 eV), oleylamine (−0.76 eV), and oleic acid ligands (−0.39 eV); (h) electrostatic potential distribution in the CNT2T molecule.

(Figure 1a). We implement this concept using a molecule having a backbone containing a triazine group (for electron mobility) and a star-shaped structure (for bending) to enable passivation from independent cyano groups to suppress traps in the InP/ZnSe/ZnS core−shell structure. The binding of CN to uncoordinated Zn^{2+} surface states enables passivation and prevents S-vacancy migration and O-vacancy formation. In this work, we implement, for the first time, local *in situ* passivation using an ETL in InP LEDs, which enables the highest EQE among organic-ETL-based red InP LEDs.

RESULTS AND DISCUSSION

We focused on the InP/ZnSe/ZnS core−shell quantum dots that emit pure red (620−640 nm). We used absorption and photoluminescence spectroscopy to characterize the InP/ZnSe/ZnS QDs (Figure 1b). The sharp exciton absorption peak at 616 nm suggests strong quantum confinement and uniform QD size, and the Gaussian-shaped PL peak centered at 627 nm corresponds to pure-red emission. X-ray diffraction (XRD) of the QD film shows typical InP/ZnSe/ZnS QD peaks; these peaks remain unchanged after aging in ambient conditions for 6 days (Figure 1c). High-resolution transmission electron microscopy (HRTEM) images of the QDs show an inter-QD distance of ∼10.1 nm (center-to-center distance) (Figure 1d); the distance between QDs of ∼2 nm coincides with the length of oleate ligands.[22,23]

We performed density functional theory (DFT) calculations to study the defect passivation mechanism of CNT2T ligands (Figure 1e−h). The calculated band structure of the ZnS (110) surface, the most stable surface, shows four main defects (Figure 1e): sulfur vacancies (V_S), zinc vacancies (V_{Zn}), sulfur interstitials (S_{int}), and zinc interstitials (Zn_{int}). We found that these induce deep trap states within the ZnS band gap, named D1−D5 (see partial charge densities in Figure S1 in the

https://doi.org/10.1021/jacs.2c13677
J. Am. Chem. Soc. XXXX, XXX, XXX−XXX

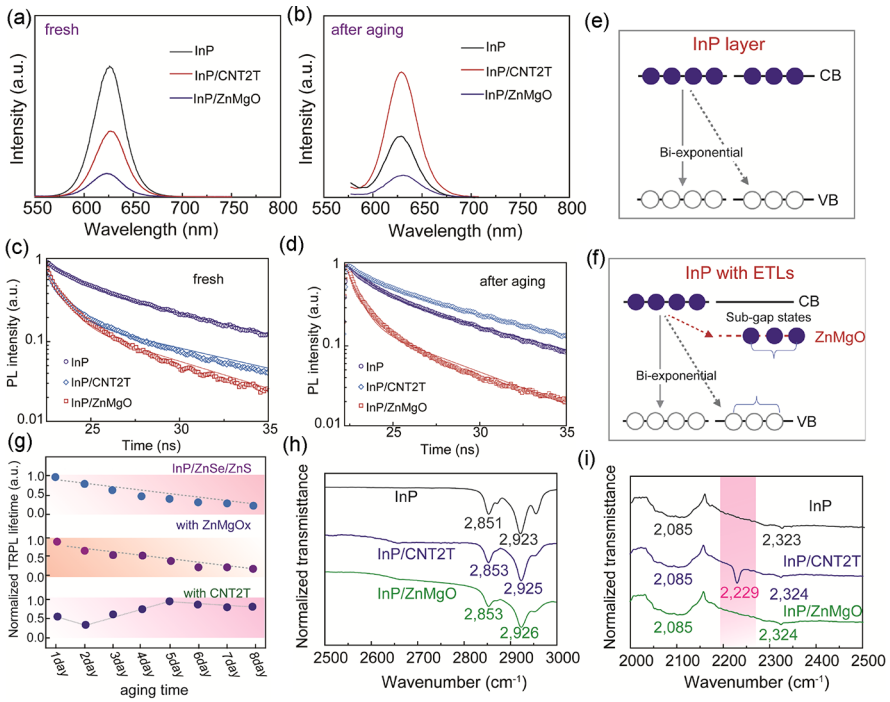

Figure 2. Steady-state and time-dependent spectroscopy of InP films with a CNT2T or ZnMgO ETL. (a, b) Photoluminescence of fresh InP, InP/CNT2T, and InP/ZnMgO films before and after aging conditions (the films were kept in the N_2-filled glovebox); (c, d) TRPL of fresh InP, InP/CNT2T and InP/ZnMgO films (c) and after aging conditions (d); (e, f) scheme showing the dynamics of pure InP films vs InP/ETLs; (g) TRPL study showing the aging trend of InP, InP/ZnMgO, and InP/CNT2T films; (h, i) Fourier-transform infrared spectroscopy (FTIR) of InP, InP/CNT2T, and InP/ZnMgO films.

Supporting Information). The previous literature[24] showed that V_S and V_{Zn} have lower defect formation energy than S_{int} and Zn_{int}, indicating that V_S and V_{Zn} are two dominant defects in ZnS. After introducing CNT2T (synthesis details of CNT2T in the Supporting Information) ligands on the ZnS surface, the formation energies of these four defects were increased (Figure 1f). CNT2T has the strongest passivation effect on sulfur vacancies V_S, as evidenced by a 0.65 eV increase in defect formation energy.

We compared the binding energy (E_b) of CNT2T and the original ligands (oleylamine and oleic acid) on an InP/ZnSe/ZnS surface with Zn^{2+} defects. The E_b of CNT2T is 1.2-fold than that of oleylamine and 2.3-fold higher than oleic acid ligands (Figure 1g). Stronger binding to these traps makes the InP surface more stable and suggests that CNT2T might actively replace the original ligands in ambient conditions or under operation and increase trap passivation. Looking at the electrostatic potential of CNT2T, we see that the CN groups at each corner are electron-rich and could interact strongly with uncoordinated Zn^{2+} (Figure 1h and Figure S2). The nonplanar structure of CNT2T results in two CN units approaching the ZnS surface, providing the means for dual-site passivation by one molecule (Figure 1g and Figure S3).

We use time-correlated single-photon counting (TCSPC) and PL spectroscopy to study the trap state density of pure InP films, compared with InP /ETL stacked films (Figure 2a–d). Fresh InP films show stronger PL intensity than either of the inorganic or organic ETL-capped films resulting from recombination at the newly formed interfaces (Figure 2a,b). However, after aging in a N_2 glovebox (5 days), the InP films capped with CNT2T show a drastic increase in PL intensity to become the brightest of the three films post-aging. The InP-only films show an average TRPL lifetime of 10.8 ns. The decay lifetime reduced to 7.2 and 9.5 ns once coated with ZnMgO and CNT2T, respectively (Figure 2c–e). This reduction in lifetime is consistent with a PLQY drop for the InP-only film (68%) to 49 and 57% for InP/ZnMgO and InP/CNT2T films, respectively. After aging, the InP and InP /ZnMgO films show a reduced lifetime of 9.8 and 6.1 ns (compared to fresh films), which we attribute to Zn^{2+} trap formation (Figure 2d). By contrast, InP /CNT2T films show an enhanced average lifetime from 9.5 to 11.2 ns, with a PLQY of 74%. This agrees with the DFT results that predicated that CNT2T provides passivation to the Zn^{2+} traps on the ZnS surface of InP.

We investigated the aging effect by measuring TRPL decay lifetime on a daily basis (up to 8 days) (Figure 2g). The InP and InP/ZnMgO films show a linear reduction in TRPL lifetime, resulting from trap formation over time. This has been observed previously, explaining that the positive aging of InP/ZnMgO LEDs only occurs when there is an Al layer (without Al, no positive aging).[25] By contrast, the InP/CNT2T film initially shows a fast TRPL lifetime decay, which gradually increases to reach a peak after 5 days of aging, from which point the TRPL remains at a similar level. This trend suggests that CNT2T may need time to passivate the InP via a quasi-solid-state ligand exhange.[26]

We use Fourier-transform infrared spectroscopy (FTIR) to characterize the three films: all the films exhibited peaks related to the C–H stretching vibrations of the methyl group (CH_3) at 2955 cm^{-1} and of the methylene group (CH_2) at 2925 and 2853 cm^{-1} (Figure 2h), whereas InP/CNT2T films have a peak at 2229 cm^{-2}, typical for the C≡N stretch (Figure 2i).

To provide insight into the InP/ZnSe/ZnS QD composition change after ETL deposition, we used cross-sectional transmission electron microscopy (TEM) and energy dispersive X-

https://doi.org/10.1021/jacs.2c13677
J. Am. Chem. Soc. XXXX, XXX, XXX–XXX

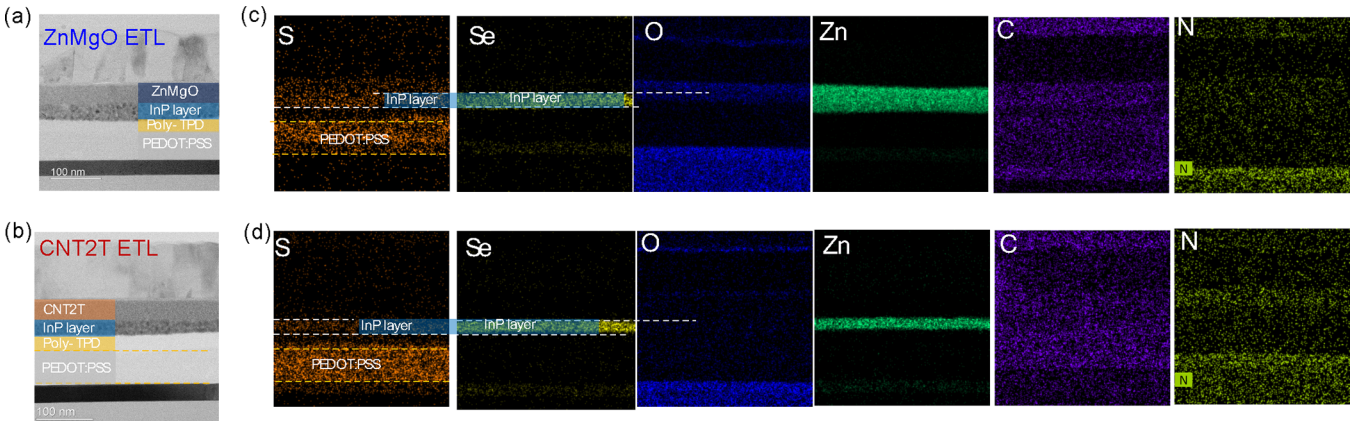

Figure 3. Effect of using the CNT2T ETL on the InP/ETL interface. (a, b) Cross-sectional TEM of InP LEDs (after aging) with ZnMgO ETL (a) and CNT2T (ETL); (c, d) EDX mapping of sulfur (S), selenium (Se), oxygen (O), zinc (Zn) carbon (C), and nitrogen (N) of InP LEDs with ZnMgO ETL (c) and CNT2T ETL (d).

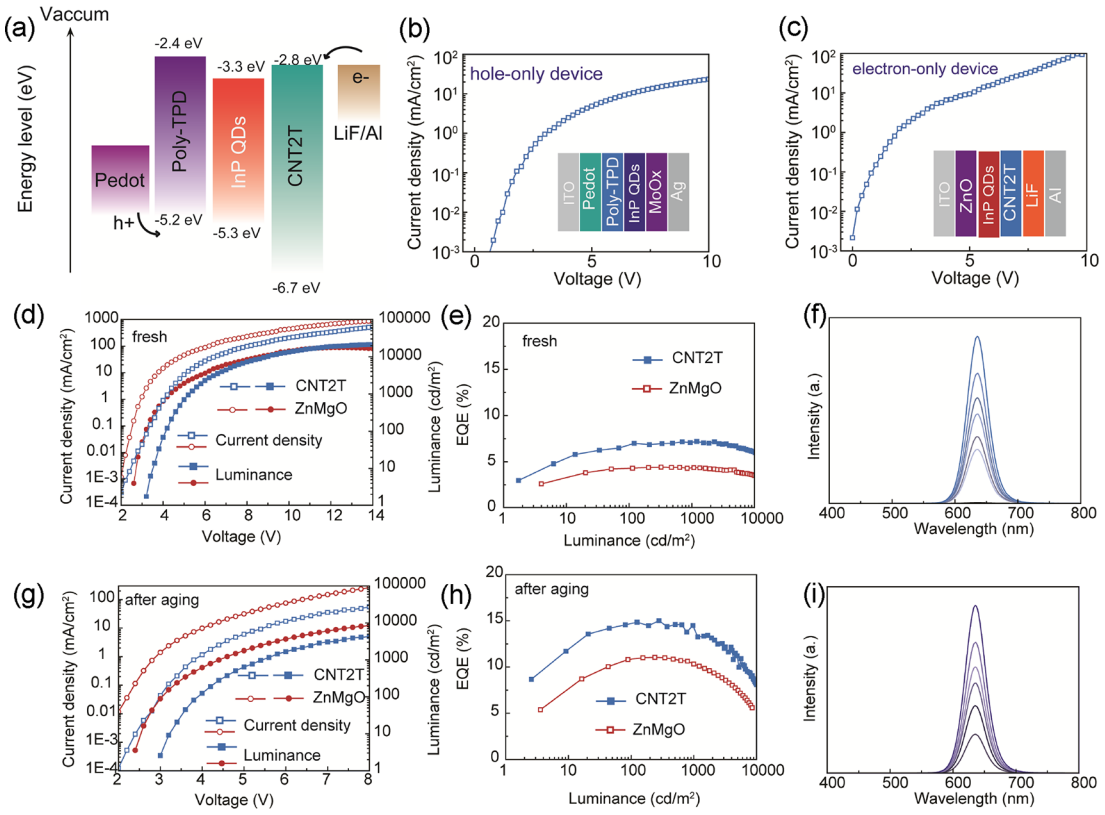

Figure 4. LED performance. (a) Band diagram of a CNT2T device. (b, c) Current density versus voltage curves of hole- (b) and electron-only (c) devices with an InP/ZnSe/ZnS QD emitter and CNT2T ETL. (d–f) Current density–voltage–luminance (d), EQE versus current density (e), and electroluminescence curves (f) of fresh devices based on CNT2T and ZnMgO ETLs. (g–i) Current density and luminance curves (g), EQE versus current density (h), and electroluminescence curves (i) of CNT2T ETL after aging.

ray spectroscopy (EDX) mapping to investigate the S and O distribution and migration after aging (Figure 3). We fabricate LEDs to compare the difference in elemental distribution between the active layer and the ETLs. Cross-sectional TEM shows a 2–3-layer stacking of the InP, suggesting an active layer thickness of ∼30 nm (Figure 3a,b), and this coincides with the thickness determined by the selenium (Se) distribution in the EDX mapping. LEDs using ZnMgO as an ETL show S and O distribution in the mixed emitter and ETL, suggesting that S migrates from the InP to the ETL layer and O vacancy of the ETL enters the InP active layer (Figure 3c), and the Zn distribution coincides with the overall O and Se distribution. In contrast, the S distribution inside LEDs with the CNT2T ETL is situated in the InP only, which does not contain any observable O signal (Figure 3d), indicating a well-passivated and protected InP. C and N are distributed substantially uniformly throughout the entire stack (except that they are absent in the Al layer) for both CNT2T and ZnMgO-based LEDs. The EDX mapping, PL decay, and DFT results together confirm that the CNT2T ETL layer passivates traps *in situ* and protects the InP surface from degradation with aging time.

https://doi.org/10.1021/jacs.2c13677
J. Am. Chem. Soc. XXXX, XXX, XXX−XXX

We next studied the suitability of CNT2T as an ETL in InP/ZnSe/ZnS LEDs by investigating the band alignment and carrier balance (Figure 4a–c). Hole-only and electron-only devices show similar hole-transport and electron-transport behavior in single-carrier devices: CNT2T shows decent electron mobility of (5.8×10^{-4} cm^2 V^{-1} s^{-1}) (Figure 4b,c); ultraviolet photoelectron spectroscopy (UPS) indicates that the conduction band of CNT2T aligns well with the InP/ZnSe/ZnS QDs (Figure S4).

Encouraged by these findings, we sought to apply the organic ETL in QD LEDs. We used a device configuration consisting of indium tin oxide (ITO as the anode, ∼32 nm)/poly(3,4-ethylenedioxythiophene)polystyrene sulfonate doped with Nafion perfluorinated ionomer (PEDOT:PSS:PFI as the hole-injection layer, ∼55 nm)/poly(4-butyl-*N*,*N*-diphenylaniline) (poly-TPD as the hole-transport layer, ∼24 nm)/InP/ZnSe/ZnS (active layer, ∼30 nm)/3′,3′″,3′″″-(1,3,5-triazine-2,4,6-triyl)tris(([1,1′-biphenyl]-3-carbonitrile)) (CNT2T as the electron-transport layer, ∼40 nm)/lithium fluoride (LiF as the electron-injection layer, ∼1 nm)/aluminum (Al as the cathode, ∼150 nm) (Figure 4a). The thickness of each functional layer was measured using cross-sectional TEM.

The LEDs using CNT2T and ZnMgO ETLs showed bright, pure-red emission (EL peak of 635 nm with a full width at half maximum of 38 nm) with similar current–voltage characteristics, though CNT2T-based devices show enhanced maximum luminance (Figure 4d). Fresh LEDs with CNT2T ETL showed a little higher EQE (∼6%) than the value achieved by using ZnMgO as the ETL (4.5%) (Figure 4e,f), while the same batch of LEDs with CNT2T after aging showed a 1.4-fold relative improvement to aged ZnMgO-ETL based LEDs (11%) and achieved a champion EQE of ∼15% (Figure 4g–i). This EQE is the highest among previously reported organic-ETL-based red InP-based QD LEDs.[11,12,20] The severe efficiency roll-off of these LEDs is attributed to a thin active layer (∼30 nm) and high electric field across the emissive layer.[27,28] The CNT2T-ETL-based InP QD LEDs have an operating lifetime (T65) of 38 h (voltage of 4 V), while the ZnMgO-ETL-based devices that used the same QDs have a T50 of 26 h under the same conditions (Figure S5).

CONCLUSIONS

In summary, we report a bifunctional ETL that enabled the highest performance organic-ETL-based red InP-based LEDs with a maximum luminance of 12,000 cd m^{-2}. The *in situ* passivation and protection of CN groups in the organic ETL provides a 1.4-fold EQE improvement compared to ZnMgO controls. Combined theoretical and experimental results suggest that CNT2T prevents the S^- migration and oxygen vacancy formation during LED operation. This work provides a new vision of ETL development and an opportunity to develop more suitable multifunction ETLs.

ASSOCIATED CONTENT

Supporting Information

The Supporting Information is available free of charge at https://pubs.acs.org/doi/10.1021/jacs.2c13677.

Additional experimental details, materials, and methods, including synthesis of InP/ZnSe/ZnS quantum dots, details on DFT calculations, UPS, and operational stability of LEDs (PDF)

AUTHOR INFORMATION

Corresponding Author

Edward H. Sargent − *Department of Electrical and Computer Engineering, University of Toronto, Toronto, Ontario M5S 3G4, Canada;* orcid.org/0000-0003-0396-6495; Email: ted.sargent@utoronto.ca

Authors

Ya-Kun Wang − *Department of Electrical and Computer Engineering, University of Toronto, Toronto, Ontario M5S 3G4, Canada; Jiangsu Key Laboratory for Carbon-Based Functional Materials & Devices, Institute of Functional Nano & Soft Materials (FUNSOM), Soochow University, Suzhou, Jiangsu 215123, PR China;* orcid.org/0000-0002-8970-6856

Haoyue Wan − *Department of Electrical and Computer Engineering, University of Toronto, Toronto, Ontario M5S 3G4, Canada;* orcid.org/0000-0001-8137-9152

Jian Xu − *Department of Electrical and Computer Engineering, University of Toronto, Toronto, Ontario M5S 3G4, Canada;* orcid.org/0000-0002-1532-5145

Yun Zhong − *Department of Materials Science and Engineering, University of Toronto, Toronto, Ontario M5S 3E4, Canada*

Eui Dae Jung − *Department of Electrical and Computer Engineering, University of Toronto, Toronto, Ontario M5S 3G4, Canada;* orcid.org/0000-0003-4848-0931

So Min Park − *Department of Electrical and Computer Engineering, University of Toronto, Toronto, Ontario M5S 3G4, Canada*

Sam Teale − *Department of Electrical and Computer Engineering, University of Toronto, Toronto, Ontario M5S 3G4, Canada;* orcid.org/0000-0001-9638-3453

Muhammad Imran − *Department of Electrical and Computer Engineering, University of Toronto, Toronto, Ontario M5S 3G4, Canada;* orcid.org/0000-0001-7091-6514

You-Jun Yu − *Jiangsu Key Laboratory for Carbon-Based Functional Materials & Devices, Institute of Functional Nano & Soft Materials (FUNSOM), Soochow University, Suzhou, Jiangsu 215123, PR China*

Pan Xia − *Department of Electrical and Computer Engineering, University of Toronto, Toronto, Ontario M5S 3G4, Canada*

Yu-Ho Won − *Samsung Electronics, Samsung Advanced Institute of Technology, Suwon-si, Gyeonggi-do 16678, Republic of Korea;* orcid.org/0000-0002-6065-7800

Kwang-Hee Kim − *Samsung Electronics, Samsung Advanced Institute of Technology, Suwon-si, Gyeonggi-do 16678, Republic of Korea*

Zheng-Hong Lu − *Department of Materials Science and Engineering, University of Toronto, Toronto, Ontario M5S 3E4, Canada;* orcid.org/0000-0003-2050-0822

Liang-Sheng Liao − *Jiangsu Key Laboratory for Carbon-Based Functional Materials & Devices, Institute of Functional Nano & Soft Materials (FUNSOM), Soochow University, Suzhou, Jiangsu 215123, PR China;* orcid.org/0000-0002-2352-9666

Sjoerd Hoogland − *Department of Electrical and Computer Engineering, University of Toronto, Toronto, Ontario M5S 3G4, Canada;* orcid.org/0000-0002-3099-585X

Complete contact information is available at: https://pubs.acs.org/10.1021/jacs.2c13677

Author Contributions

[#]Y.-K.W., H.W., J.X., and Y.Z. contributed equally.

Notes

The authors declare no competing financial interest.

■ ACKNOWLEDGMENTS

This work was supported by Samsung Electronics Co. (MRA 211815). We acknowledge financial support from the Natural Science Foundation of China (nos. 62205230, 51821002, 91733301), China Postdoctoral Science Foundation (2021TQ0230, 2021M690114), and the Collaborative Innovation Center of Suzhou Nano Science and Technology. Computations were performed on the Niagara supercomputer at the SciNet HPC Consortium. SciNet is funded by the Canada Foundation for Innovation, the Government of Ontario, and the University of Toronto.

■ REFERENCES

(1) Arquer, F. P. G. D.; et al. Semiconductor quantum dots: Technological progress and future challenges. *Science* **2021**, *373*, No. eaaz8541.
(2) Shirasaki, Y.; Supran, G. J.; Bawendi, M. G.; Bulović, V. Emergence of colloidal quantum-dot light-emitting technologies. *Nat. Photonics* **2013**, *7*, 13.
(3) Han, M. G.; et al. InP-Based Quantum Dot Light-Emitting Diode with a Blended Emissive Layer. *ACS Energy Lett.* **2021**, *6*, 1577.
(4) Deng, Y.; et al. Solution-processed green and blue quantum-dot light-emitting diodes with eliminated charge leakage. *Nat. Photon.* **2022**, *16*, 505.
(5) Pradhan, S.; et al. High-efficiency colloidal quantum dot infrared light-emitting diodes via engineering at the supra-nanocrystalline level. *Nat. Nanotechnol.* **2019**, *14*, 72.
(6) Caruge, J. M.; Halpert, J. E.; Wood, V.; Bulović, V.; Bawendi, M. G. Colloidal quantum-dot light-emitting diodes with metal-oxide charge transport layers. *Nat. Photonics* **2008**, *2*, 247.
(7) Shen, H.; et al. High-Efficiency, Low Turn-on Voltage Blue-Violet Quantum-Dot-Based Light-Emitting Diodes. *Nano Lett.* **2015**, *15*, 1211.
(8) Mashford, B. S.; Stevenson, M.; Popovic, Z.; Hamilton, C.; Zhou, Z.; Breen, C.; Steckel, J.; Bulovic, V.; Bawendi, M.; Coe-Sullivan, S.; Kazlas, P. T. High-efficiency quantum-dot light-emitting devices with enhanced charge injection. *Nat. Photonics* **2013**, *7*, 407.
(9) Won, Y.-H.; et al. Highly efficient and stable InP/ZnSe/ZnS quantum dot light-emitting diodes. *Nature* **2019**, *575*, 634.
(10) Wu, Z.; et al. Development of InP Quantum Dot-Based Light-Emitting Diodes. *ACS Energy Lett.* **2020**, *5*, 1095.
(11) Iwasaki, Y.; et al. Efficient green InP quantum dot light-emitting diodes using suitable organic electron-transporting materials. *Appl. Phys. Lett.* **2020**, *117*, 111104.
(12) Choi, H.-S.; et al. Enhanced Electroluminescence via a Nanohybrid Material Consisting of Aromatic Ligand-Modified InP Quantum Dots and an Electron-Blocking Polymer as the Single Active Layer in Quantum Dot-LEDs. *Nanomaterials* **2022**, *12*, 408.
(13) Kim, H. Y.; Park, Y. J.; Kim, J.; Han, C. J.; Lee, J.; Kim, Y.; Greco, T.; Ippen, C.; Wedel, A.; Ju, B. K.; Oh, M. S. Transparent InP Quantum Dot Light-Emitting Diodes with ZrO2 Electron Transport Layer and Indium Zinc Oxide Top Electrode. *Adv. Funct. Mater.* **2016**, *26*, 3454.
(14) Yoo, J.-Y.; et al. Efficient InP/ZnSe/ZnS quantum dot shelling and the effect of a bi-layered organic-inorganic electron-transport layer on the performance of quantum dot light-emitting diode devices. *Org. Electron.* **2022**, *108*, No. 106569.
(15) Chen, Z.; Chen, S. Efficient and Stable Quantum-Dot Light-Emitting Diodes Enabled by Tin Oxide Multifunctional Electron Transport Layer. *Adv. Opt. Mater.* **2022**, *10*, No. 2102404.
(16) Zaiats, G.; Ikeda, S.; Kamat, P. V. Optimization of the electron transport layer in quantum dot light-emitting devices. *NPG Asia Mater.* **2020**, *12*, 57.
(17) Cao, Y.; et al. Perovskite light-emitting diodes based on spontaneously formed submicrometre-scale structures. *Nature* **2018**, *562*, 249.
(18) Xu, W.; Hu, Q.; Bai, S.; Bao, C.; Miao, Y.; Yuan, Z.; Borzda, T.; Barker, A. J.; Tyukalova, E.; Hu, Z.; Kawecki, M.; Wang, H.; Yan, Z.; Liu, X.; Shi, X.; Uvdal, K.; Fahlman, M.; Zhang, W.; Duchamp, M.; Liu, J. M.; Petrozza, A.; Wang, J.; Liu, L. M.; Huang, W.; Gao, F. Rational molecular passivation for high-performance perovskite light-emitting diodes. *Nat. Photonics* **2019**, *13*, 418.
(19) Yuan, Z.; et al. Unveiling the synergistic effect of precursor stoichiometry and interfacial reactions for perovskite light-emitting diodes. *Nat. Commun.* **2019**, *10*, 2818.
(20) Yang, L.; et al. High-Performance Red Quantum-Dot Light-Emitting Diodes Based on Organic Electron Transporting Layer. *Adv. Funct. Mater.* **2021**, *31*, No. 2007686.
(21) Gao, P.; Zhang, Y.; Qi, P.; Chen, S. Efficient InP Green Quantum-Dot Light-Emitting Diodes Based on Organic Electron Transport Layer. *Adv. Opt. Mater.* **2022**, *10*, No. 2202066.
(22) Wang, Y.-K.; Yuan, F.; Dong, Y.; Li, J. Y.; Johnston, A.; Chen, B.; Saidaminov, M. I.; Zhou, C.; Zheng, X.; Hou, Y.; Bertens, K.; Ebe, H.; Ma, D.; Deng, Z.; Yuan, S.; Chen, R.; Sagar, L. K.; Liu, J.; Fan, J.; Li, P.; Li, X.; Gao, Y.; Fung, M. K.; Lu, Z. H.; Bakr, O. M.; Liao, L. S.; Sargent, E. H. All-Inorganic Quantum-Dot LEDs Based on a Phase-Stabilized α-CsPbI3 Perovskite. *Angew. Chem., Int. Ed.* **2021**, *60*, 16164.
(23) Dong, Y.; et al. Bipolar-shell resurfacing for blue LEDs based on strongly confined perovskite quantum dots. *Nat. Nanotechnol.* **2020**, *15*, 668.
(24) Varley, J. B.; Lordi, V. Electrical properties of point defects in CdS and ZnS. *Appl. Phys. Lett.* **2013**, *103*, 102103.
(25) Su, Q.; et al. Origin of Positive Aging in Quantum-Dot Light-Emitting Diodes. *Adv. Sci.* **2018**, *5*, No. 1800549.
(26) Kirmani, A. R.; et al. Optimizing Solid-State Ligand Exchange for Colloidal Quantum Dot Optoelectronics: How Much Is Enough? *ACS Appl. Energy Mater.* **2020**, *3*, 5385.
(27) Zou, W.; et al. Minimising efficiency roll-off in high-brightness perovskite light-emitting diodes. *Nat. Commun.* **2018**, *9*, 608.
(28) Liang, Y.; et al. Lasing from Mechanically Exfoliated 2D Homologous Ruddlesden−Popper Perovskite Engineered by Inorganic Layer Thickness. *Adv. Mater.* **2019**, *31*, No. 1903030.

https://doi.org/10.1021/jacs.2c13677
J. Am. Chem. Soc. XXXX, XXX, XXX−XXX